



Solidification cracking in duplex stainless steel flux-cored arc welds Part 2 — susceptibility of 22Cr all-weld metals under high restraint

Elin M. Westin¹ · Fernando G. Warchomicka²

Received: 23 July 2022 / Accepted: 22 September 2022 / Published online: 7 October 2022
© International Institute of Welding 2022

Abstract

Due to their high strength and corrosion resistance, duplex stainless steels are increasingly used in applications where heavy-wall material is welded under highly restrained conditions. Despite the ferritic solidification and experience shared in most available literature, these alloys are not immune to hot cracking. In this work, different commercial and experimental flux-cored wires of E2209T0 and E2209T1 type were subject to flux-cored arc welding (FCAW) to evaluate the susceptibility to solidification cracking. Impact toughness testing of all-weld metal on restrained plates proved an efficient method to detect and inspect cracks by examining the fracture surfaces. Particles found in cracks and dimples were characterized by means of scanning electron microscopy (SEM) and energy-dispersive X-ray spectroscopy (EDS). While the start of the observed cracks showed a classic dendritic or dendritic-flat solidification pattern, the end with the last solidified melt was rather smooth. Examination in backscatter mode clearly visualized bismuth to be present in the flat region adhering to manganese sulfide (MnS) particles. Cracks were, however, also detected with bismuth-free wires and wires with low sulfur content. The weld metal chemical composition, source of raw materials, and selected agents for deoxidation could play an important role, while certain formulations with special concepts for slag formation may be less susceptible. The E2209T1 types with more rapidly solidifying slag generally showed higher resistance to solidification cracking than the E2209T0 wires, which also contained substantially higher total amounts of sulfur, phosphorous, boron, oxygen, and bismuth.

Keywords Duplex stainless steel · FCAW · Solidification cracking · Low-melting phases · Impurities

1 Introduction

The modern duplex stainless steels have overall good weldability, and the range of possible applications has increased. The combination of high strength and corrosion resistance was traditionally utilized in the offshore and pulp and paper industries, but have gained use in general construction, bridge building, and production of chemical tankers. The new generations of duplex grades contain more nitrogen, which has increased the strength and improved the

weldability by promoting austenite formation [1]. Increased wall thickness, strength, and high restraint when welding can lead to higher strain and strain rates [2, 3]. With fully ferritic solidification, the duplex alloys are usually considered to have high resistance to solidification cracking [4]. The ferrite has higher solubility and diffusivity for impurities than austenite so the grain boundary concentration is lower [5, 6]. Impurity elements can originate from both from the parent material and filler metal additions.

Most published papers on hot cracking included older materials with lower amounts of nitrogen and showed an intermediate cracking susceptibility between austenitic stainless steels with ferritic and fully austenitic solidification, respectively [7, 8]. Cracking in duplex plates above 10 mm thickness have been observed with the shielded metal arc welding (SMAW), gas metal arc welding (GMAW), and submerged arc welding (SAW) processes [9, 10]. Particularly sulfur and phosphorus promote hot cracking by lowering the solidus temperature and lengthening the brittle temperature range [11–13].

Recommended for publication by Commission IX - Behaviour of Metals Subjected to Welding.

✉ Elin M. Westin
elin.westin@voestalpine.com

¹ voestalpine Böhler Welding Austria GmbH,
Böhler-Welding-Str. 1, 8605 Kapfenberg, Austria

² Institute of Materials Science, Joining and Forming, Graz
University of Technology, 8010 Graz, Austria

Saida and Ogura [14] studied modern alloys with gas tungsten arc welding (GTAW) and laser welding, and concluded that lean, standard, and super duplex were as resistant as austenitic stainless steels solidifying in ferritic-austenitic (FA) mode. Suppression of segregated phosphorous, sulfur, and carbon was suggested to have improved the cracking resistance as compared to austenitic alloys with austenitic-ferritic (AF) or fully austenitic (A) solidification. Hot cracking has also been observed for UNS S32205 material welded with the SAW, laser, and laser hybrid processes where the ferrite content was high or the weld bead shape was very thin [15, 16]. The problem could be avoided after adjustment of the parameters to allow for more austenite formation and an optimum weld bead shape.

In a ranking of the relative laser weldability of 11 different austenitic, superaustenitic, and duplex stainless grades with the controlled tensile weldability (CTW) test, the austenitic AISI 301LN alloy and the lean duplex grades UNS S32101 and UNS S32304 showed the highest resistance to cracking [17]. The standard duplex UNS S32205 was, on the other hand, suggested to be somewhat more susceptible than AISI 304L and AISI 316L, which solidified in the FA mode.

Steel suppliers and wire manufacturers are aware of a few other cases where solidification cracks have been found in duplex stainless steels, but it is unclear how much of this experience has been published. A more detailed review can be found in an earlier work [18]. Some duplex flux-cored wire formulations have been claimed to cause solidification cracking when welding thick-walled material. In Part 1 of this paper series [19], three wires from different manufacturers produced in 2005, 2011, and 2016 were confirmed to cause formation of solidification cracks when welding 30-mm-thick UNS S32101 and UNS S32205. Cracks were observed to propagate in the long and straight ferrite grain boundaries, where low-melting phases containing sulfur and bismuth were liquid when subject to critical strain. A wire intended for welding in all welding positions was concluded to be more resistant and it was suggested to further investigate the effect of impurities and different slag types on cracking susceptibility. In this work, Part 2, all-weld metals of E2209T0 and E2209T1 type were welded under full restraint to study the effect of the chemical composition and slag concept only. The goal was to evaluate if these types of wires available on the market are susceptible to solidification cracking or not.

2 Experimental

The investigated \varnothing 1.2 mm E2209 duplex stainless steel flux-cored wires had dual classification for welding with both mixed gas Ar + 18–25% CO₂ (M21) and 100% CO₂ (C1). Nineteen wires were intended for welding in best

position (T0) and 19 for welding in all positions (T1). EN ISO 17633-A [20] separates these types of wires as R and P, respectively. The wires originated from five different manufacturers. The chemical composition is shown in Table 1. The wires E2209T1-M to E2209T1-S were bismuth-free with less than 0.0002 wt.-% bismuth.

All-weld metal was produced using EN 15792–1 [21] selecting the 1.3 test piece type (Fig. 1). The base material was 20-mm-thick unalloyed steel with 10° beveling and the gap was 16 mm. Both the backing and plate groove edges were buttered with two layers using the same wire being tested. The plates were clamped with transversely welded plates to maintain a condition of high restraint and preheated to 100 °C. Manual welding was carried out in the flat position (PA/1G) using the FCAW process with the parameters listed in Table 2. If residuals were present on the surface after the slag had been detached, these were removed with a grinding wheel. The ferrite content was measured on five locations on the final weld bead using a Fischer Feritescope® MP30. The surface of the weld metal was manually prepared using a single cut flat file in accordance with EN ISO 17655 [22].

Impact toughness testing was carried out on five full-size Charpy-V 10 × 10 × 55 mm specimens in all-weld metals according to ISO 148–1 [23]. The samples were taken from the center of the welded plate and the notch placed in the midpoint of the weld (Fig. 2). Testing was performed at room temperature and at –40 °C. The fracture surfaces were examined with scanning electron microscopy (SEM) and the size of any observed solidification cracks was measured. The instrument used was a TESCAN Mira3 (TESCAN, Brno, Czech Republic) microscope equipped with an energy-dispersive X-ray spectroscopy (EDS) Super Octane detector with a 60 mm² active area (EDAX AMETEK, Mahwah, NJ, USA).

3 Results

3.1 Impact toughness, ferrite measurements, and visual examination of fracture surfaces

The results from the impact toughness testing and the ferrite measurement as FN in the last weld bead are shown in Table 3. The impact toughness was highest for the wires intended for welding in all positions and only a few wires showed indications of weld cracking on the fracture surface. Contrarily, more than half of the E2209T0 wires showed evidence of cracking. The range of ferrite numbers measured with the FeriteScope® was rather wide, 31–64 FN, but there was not a large difference between the E2209T0 and E2209T1 wires.

Table 1 All-weld metal composition of flux-cored wires welded with Ar + 18% CO₂, wt.-%

Wire	C	Si	Mn	P	S	Cr	Ni	Mo	Cu	N	Bi	B	WRC '92, FN
E2209T0-A	0.029	0.68	0.93	0.023	0.006	22.8	8.84	3.09	0.17	0.16	0.004	0.0015	41
E2209T0-B	0.027	0.70	0.92	0.023	0.004	22.9	8.74	3.08	0.17	0.17	0.003	0.0016	41
E2209T0-C	0.024	0.71	0.94	0.022	0.004	22.9	8.60	3.19	0.12	0.16	0.003	0.0022	48
E2209T0-D	0.021	0.73	0.96	0.024	0.005	22.6	8.93	3.13	0.12	0.14	0.006	0.0028	45
E2209T0-E	0.024	0.67	0.92	0.023	0.004	22.7	9.17	3.20	0.17	0.15	0.004	0.0023	42
E2209T0-F	0.020	0.71	0.94	0.022	0.007	23.0	8.97	3.32	0.12	0.14	0.003	0.0032	52
E2209T0-G	0.023	0.69	0.93	0.022	0.006	22.5	8.72	3.19	0.13	0.13	0.002	0.0028	51
E2209T0-H	0.026	0.70	0.77	0.021	0.005	22.2	8.65	3.02	0.14	0.15	0.005	0.0023	40
E2209T0-I	0.027	0.70	0.74	0.022	0.004	22.0	8.81	3.11	0.13	0.14	0.006	0.0025	38
E2209T0-J	0.031	0.69	0.72	0.021	0.003	22.3	8.68	3.13	0.13	0.16	0.003	0.0022	36
E2209T0-K	0.024	0.58	0.90	0.024	0.005	22.4	9.11	3.01	0.13	0.13	0.007	0.0022	40
E2209T0-L	0.028	0.64	0.86	0.023	0.004	22.6	8.63	3.27	0.13	0.15	0.005	0.0028	45
E2209T0-M	0.026	0.61	0.92	0.021	0.005	22.7	9.15	3.28	0.13	0.14	0.005	0.0050	43
E2209T0-N	0.026	0.63	0.91	0.021	0.004	22.6	9.37	3.42	0.13	0.14	0.006	0.0026	42
E2209T0-O	0.024	0.59	0.90	0.020	0.004	22.4	9.30	3.13	0.13	0.13	0.004	0.0021	39
E2209T0-P	0.020	0.79	0.98	0.022	0.005	23.1	9.32	2.91	0.14	0.14	0.011	0.0004	45
E2209T0-Q	0.023	0.73	1.08	0.021	0.003	23.3	9.34	3.21	0.10	0.13	0.003	0.0010	53
E2209T0-R	0.028	0.51	0.90	0.018	0.003	22.6	8.83	3.02	0.07	0.13	0.002	0.0008	45
E2209T0-S	0.029	0.53	0.95	0.019	0.003	23.0	8.91	3.16	0.10	0.13	0.002	0.0007	50
E2209T1-A	0.026	0.59	1.09	0.022	0.003	22.7	9.00	3.07	0.13	0.13	0.002	0.0008	45
E2209T1-B	0.030	0.59	1.06	0.023	0.003	22.8	9.02	3.08	0.12	0.14	0.002	0.0006	44
E2209T1-C	0.027	0.59	1.09	0.022	0.003	22.9	8.86	3.19	0.12	0.14	0.002	0.0006	49
E2209T1-D	0.030	0.60	0.90	0.020	0.002	22.5	8.93	3.13	0.12	0.14	0.002	0.0006	42
E2209T1-E	0.024	0.59	1.09	0.022	0.003	22.9	9.05	3.34	0.09	0.13	0.002	0.0006	52
E2209T1-F	0.025	0.61	1.07	0.022	0.003	23.0	8.87	3.02	0.10	0.13	0.002	0.0006	52
E2209T1-G	0.031	0.60	0.87	0.021	0.003	22.1	8.80	2.92	0.12	0.13	0.002	0.0009	35
E2209T1-H	0.029	0.63	0.90	0.020	0.002	22.2	8.82	2.83	0.12	0.13	0.002	0.0007	38
E2209T1-I	0.024	0.55	1.04	0.022	0.002	23.0	8.90	3.13	0.17	0.13	0.002	0.0007	52
E2209T1-J	0.027	0.66	1.08	0.021	0.002	22.6	8.69	3.19	0.12	0.14	0.002	0.0007	35
E2209T1-K	0.027	0.69	0.93	0.020	0.002	22.6	9.00	3.12	0.09	0.13	0.002	0.0008	46
E2209T1-L	0.029	0.67	0.95	0.019	0.002	23.0	8.97	3.14	0.08	0.13	0.002	0.0005	50
E2209T1-M	0.021	0.56	0.99	0.017	0.008	23.5	8.95	3.52	0.05	0.13	<0.001	0.0006	64
E2209T1-N	0.033	0.64	0.91	0.022	0.003	22.9	8.98	3.16	0.10	0.15	<0.001	0.0006	42
E2209T1-O	0.028	0.65	0.91	0.022	0.004	22.6	9.21	3.16	0.13	0.12	<0.001	0.0007	43
E2209T1-P	0.026	0.62	0.92	0.021	0.005	22.8	9.14	3.10	0.10	0.14	<0.001	0.0006	43
E2209T1-Q	0.023	0.62	0.90	0.020	0.005	23.2	9.13	3.16	0.10	0.14	<0.001	0.0007	49
E2209T1-R	0.027	0.64	0.90	0.021	0.004	22.7	9.10	3.20	0.11	0.15	<0.001	0.0007	40
E2209T1-S	0.026	0.58	0.93	0.017	0.003	23.0	9.04	3.09	0.08	0.13	<0.001	0.0006	50

3.2 Fracture surfaces examined with SEM/EDS

Eight fracture surfaces were selected for further examination with SEM/EDS. These represented wires from different manufacturers and the cracks were sufficiently small to contain both the start and end. Four out of the eight samples displayed dendritic patterns typical for solidification cracks, as observed in Fig. 3. The approximate crack size measured for samples E2209T0-G (Fig. 3a), E2209T0-E (Fig. 3b), E2209T1-A (Fig. 3c), and E2209T1-Q (Fig. 3d)

was 0.75×1.5 , 0.86×2.0 mm, 0.98×0.7 , and 0.45×1.3 mm, respectively. Samples E2209T0-E and E2209T1-Q showed cracks in two layers indicating more than one crack in the same weld bead.

The cracks were examined at higher magnification using both secondary electron (SE) and backscatter electron (BSE) mode (Fig. 4). One side of the crack always showed dendritic solidification, while the other side was flat. With backscatter, a bright phase became visible in the flat region of the cracks found with the wires E2209T0-G (Fig. 4a),

Fig. 1 Joint preparation for creating all-weld metal for impact toughness testing

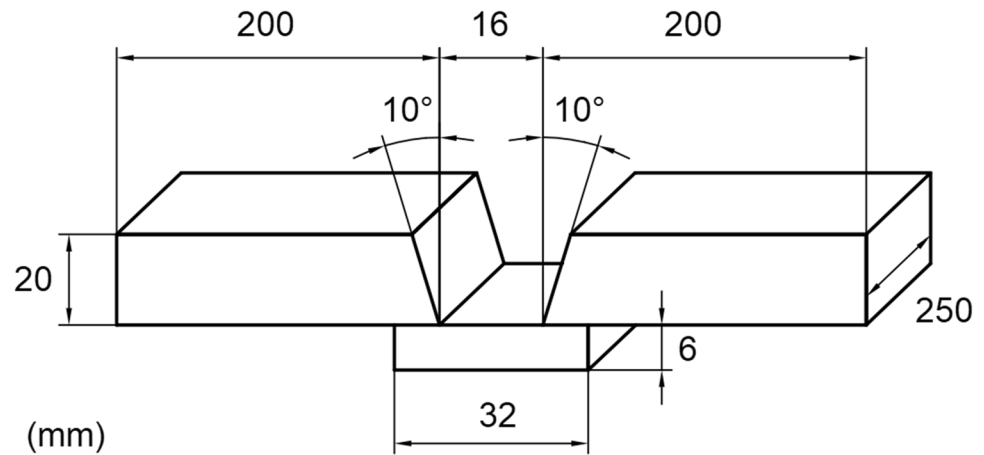


Table 2 Welding parameters

Welding machine	Fronius TR4000	Arc length	~ 3 mm
Current	220–230 A	Shielding gas	Ar + 18% CO ₂
Voltage	27–30 V	Gas flow	16–18 l/min
Wire feeding rate	12 m/min	Number of layers	7
Welding speed	0.30–0.38 m/min	Number of runs	14–15
Heat input	0.9–1.1 kJ/mm	Interpass temperature	Max. 150 °C
Wire stick-out	15–20 mm	Polarity	DC +

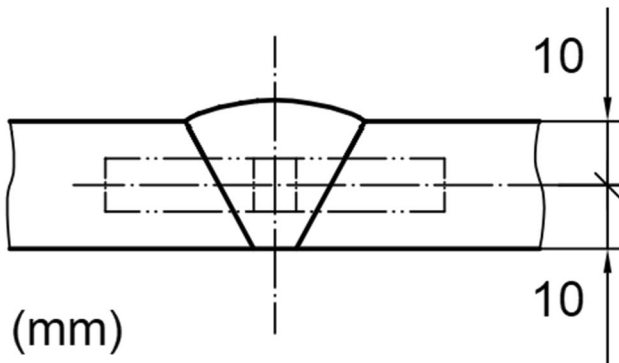


Fig. 2 Sampling location for impact toughness test pieces

E2209T0-E (Fig. 4b), and E2209T1-A (Fig. 4c). EDS analysis suggested that it consisted of predominantly bismuth with smaller amounts of iron, chromium, manganese, and sulfur. Particles found in the dimples on the fracture surface further away from the solidification cracks were rich in chromium, manganese, iron, titanium, and silicon.

An examination of the bismuth particles located in the dimples adjacent to the flat region at higher magnification revealed that bismuth was present in close proximity or as a coating of other particles (Fig. 5a–d). These had a substantial amount of manganese and sulfur, and were identified as manganese sulfides (MnS). The size was typically in the range 0.5–2 μm .

The fracture surfaces for the wires E2209T0-H and E2209T1-B were free from solidification cracks, but when examining the dimples, small areas of bismuth could also be located with backscatter on MnS particles (Fig. 6a–b). The majority of the particles in the dimples consisted of chromium, manganese, iron, silicon, and titanium oxides. Only small amounts of sulfur could be detected. Also here the size of the MnS particles was typically in the range of 0.5–2 μm .

No bismuth was found in the flat region of the solidification crack found with wire E2209T1-Q, which could be expected from the bismuth-free composition. Instead, spherical particles were observed (Fig. 7a). These were distributed along the striation lines (Fig. 7b–c), with the largest size in the dendrite and ferrite grain boundaries (Fig. 7d). EDS indicated these to be rich in manganese and silicon. Outside the crack, ductile failure could be confirmed with dimples of various sizes. Inclusions and particles of 0.1–3.0- μm size in the dimples consisted of MnS and iron, chromium, silicon, manganese, and titanium oxides.

Because of the unusual appearance, another all-weld metal sample was produced with wire E2209T1-Q, subjected to impact toughness testing, and examined for cracks. Small indications were found on four out of six fracture surfaces. Figure 8a shows a sample where the crack appeared on more layers. The surface showed dendritic-flat structure (Fig. 8b) and the end of the crack was flat (Fig. 8c). In the flat region, the surface was observed to have striations, and particles rich in manganese and

Table 3 Ferrite measurement and impact toughness, all-weld metal welded with Ar+18% CO₂

Wire	FN last bead	Impact toughness, J		Samples with cracks
		20 °C	−40 °C	
E2209T0-A	41 ± 2	56 ± 7	45 ± 1	5/10
E2209T0-B	40 ± 1	62 ± 5	43 ± 4	5/10
E2209T0-C	45 ± 1	63 ± 2	46 ± 3	2/10
E2209T0-D	43 ± 3	63 ± 2	46 ± 2	0/10
E2209T0-E	40 ± 3	64 ± 2	47 ± 1	1/10*
E2209T0-F	44 ± 1	59 ± 3	43 ± 3	2/10
E2209T0-G	50 ± 2	56 ± 2	44 ± 2	7/10*
E2209T0-H	35 ± 2	68 ± 2	47 ± 1	0/10*
E2209T0-I	40 ± 2	67 ± 2	50 ± 1	0/10
E2209T0-J	37 ± 1	69 ± 1	48 ± 1	0/10
E2209T0-K	37 ± 1	53 ± 4	40 ± 2	5/10
E2209T0-L	47 ± 1	56 ± 1	40 ± 2	3/10
E2209T0-M	46 ± 2	52 ± 3	41 ± 1	1/10
E2209T0-N	39 ± 1	56 ± 1	43 ± 2	1/10
E2209T0-O	40 ± 1	55 ± 2	41 ± 1	0/10
E2209T0-P	39 ± 2	52 ± 2	35 ± 1	0/10
E2209T0-Q	53 ± 1	67 ± 2	47 ± 2	4/10
E2209T0-R	49 ± 4	58 ± 3	47 ± 2	0/10
E2209T0-S	51 ± 2	60 ± 2	49 ± 2	0/10
E2209T1-A	47 ± 2	73 ± 3	53 ± 2	2/10*
E2209T1-B	46 ± 2	63 ± 2	52 ± 2	0/10*
E2209T1-C	48 ± 2	70 ± 2	51 ± 2	0/10
E2209T1-D	44 ± 2	77 ± 3	58 ± 1	0/10
E2209T1-E	54 ± 3	58 ± 2	49 ± 2	0/10
E2209T1-F	40 ± 1	66 ± 1	47 ± 1	0/10
E2209T1-G	44 ± 3	66 ± 2	51 ± 2	0/10
E2209T1-H	31 ± 1	72 ± 3	54 ± 2	0/10
E2209T1-I	46 ± 3	59 ± 2	48 ± 2	0/10
E2209T1-J	53 ± 4	58 ± 2	50 ± 2	0/10
E2209T1-K	52 ± 4	58 ± 2	46 ± 2	0/10
E2209T1-L	55 ± 3	62 ± 3	48 ± 3	0/10
E2209T1-M	64 ± 2	76 ± 3	51 ± 1	0/10
E2209T1-N	46 ± 4	85 ± 3	63 ± 2	0/10
E2209T1-O	42 ± 1	83 ± 2	64 ± 2	0/10
E2209T1-P	46 ± 1	84 ± 3	60 ± 1	0/10*
E2209T1-Q	46 ± 2	78 ± 3	60 ± 1	1/10*
E2209T1-R	45 ± 2	86 ± 3	64 ± 3	0/10*
E2209T1-S	45 ± 3	86 ± 1	60 ± 2	0/10

*Selected for SEM and EDS examination

silicon of approximately 0.09–1.2- μm size decorated the complete surface. The largest particles were located in the ferrite and dendrite boundaries (Fig. 8d). Close to the grain boundaries with the largest particles, there was a region slightly depleted from particles (Fig. 8e). One single bright particle consisting of essentially pure molybdenum was found (Fig. 8f).

Wires E2209T1-P and E2209T1-R did not show any solidification cracks on the fracture surfaces. The dimples primarily contained iron, chromium, manganese, silicon, and titanium oxides (Fig. 9). A difference in inclusion shape was observed, where the particles in E2209T1-P were visually somewhat larger and circular (Fig. 9a) and in E2209T1-R smaller and more irregular (Fig. 9b). Both wires showed high and similar average impact toughness.

4 Discussion

4.1 Impact toughness testing

The acceptance criteria in ISO 17781 [24] divide the minimum absorbed energy at $-46\text{ }^{\circ}\text{C}$ for duplex stainless steel in as-welded condition in two quality levels. The most common requirement, quality level QL II, is sufficient for most applications and requires a mean minimum energy of 35 J, with no sample below 27 J. Most of the wires in this work would probably pass this requirement also in a welded joint, but the joint preparation and welding conditions may affect the properties further. To fulfil the strictest quality level QL I, the minimum mean energy needed is 50 J and a minimum of 40 J for a single sample. Presumably, none of the E2209T0, while some of the E2209T1 wires, would fulfill this requirement, but it will need further investigation.

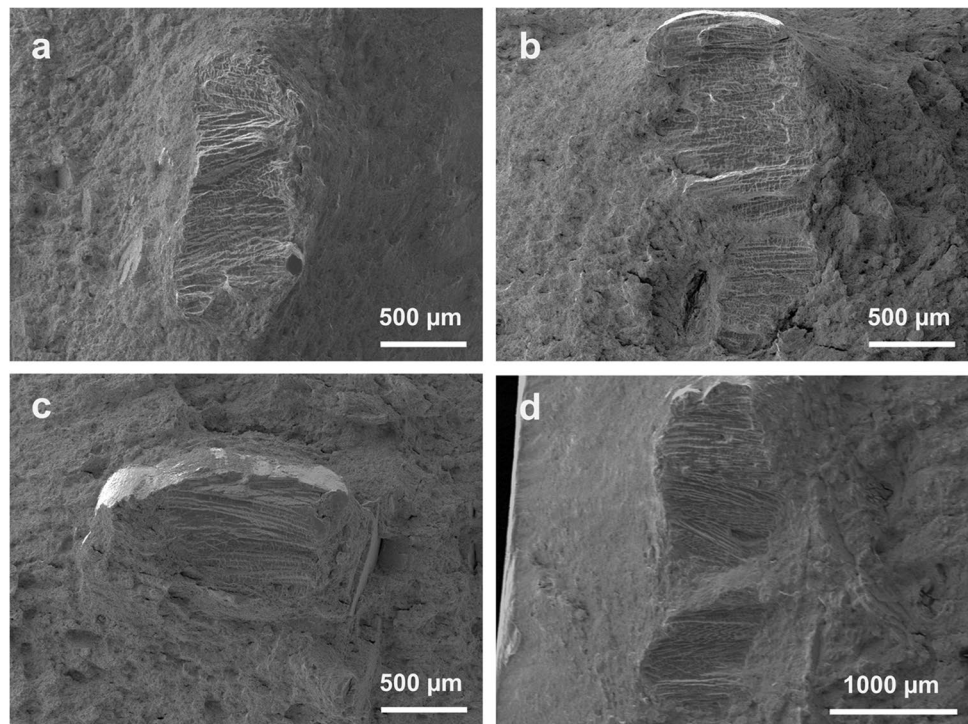
The wires developed for all welding positions generally had higher impact toughness, which is in line with the experience that these products have lower weld metal oxygen content [25–27]. The bismuth-free wires mostly showed the highest impact toughness, which could be anticipated as additions of Bi₂O₃ have a slightly negative effect on the low temperature toughness of FCAW weldments by increasing the oxygen content and resultant oxide inclusions [27–30].

Cracks were observed on the fracture surface of some of the impact toughness samples. Samples from a few wires showed up to three cracks within one surface indicating cracking in three separate weld passes. Some cracks had different steps in the surface level, which could indicate formation of more than one crack in the same weld bead.

It should be noted that this is a random sampling and that the full cross-section of the all-weld metal is not covered by the $10\times 10\text{ mm}$ area of the impact toughness samples. This means that some solidification cracks may have remained undetected.

The crack depth was typically in the range of 0.5–1.0 mm, but the length (along the weld) ranged from 0.5 mm up to the full sample width. This made it difficult to document and compare the total crack length so instead the total number of cracked samples out of ten was recorded. The number of samples displaying solidification cracks did not, however, reveal any relation to the impact toughness, but the individual samples often showed

Fig. 3 Fracture surfaces with solidification cracks observed on impact toughness samples welded with the wires. **a** E2209T0-G, **b** E2209T0-E, **c** E2209T1-A, and **d** E2209T1-Q (SE mode)



the lowest values with a reduction within the standard deviation.

The shortest cracks were generally found for the E2209T1 wires. This is in agreement with the work of Cardoso Junior et al. [31] where discontinuities smaller than 1.0 mm were found in weldments produced with flux-cored wires of E2307T1 type.

No clear correlation could be found between the observation of cracking and the impact toughness, but more samples contained cracks for the E2209T0 wires and these wires also generated the lowest toughness. The ferrite content measured in the last weld bead or calculated using the WRC'92 diagram did not have a quantifiable influence on the impact toughness.

No single element had a significant effect on the impact toughness for all wires from different manufacturers, but when combining the phosphorous, sulfur, bismuth, and boron contents, it becomes clear that the E2209T0 wires contain more of the elements known to promote hot cracking (Fig. 10). A weak trend could be seen that the toughness decreases with more impurities, but the slag concept may overshadow this effect by determining the solidification temperature and range.

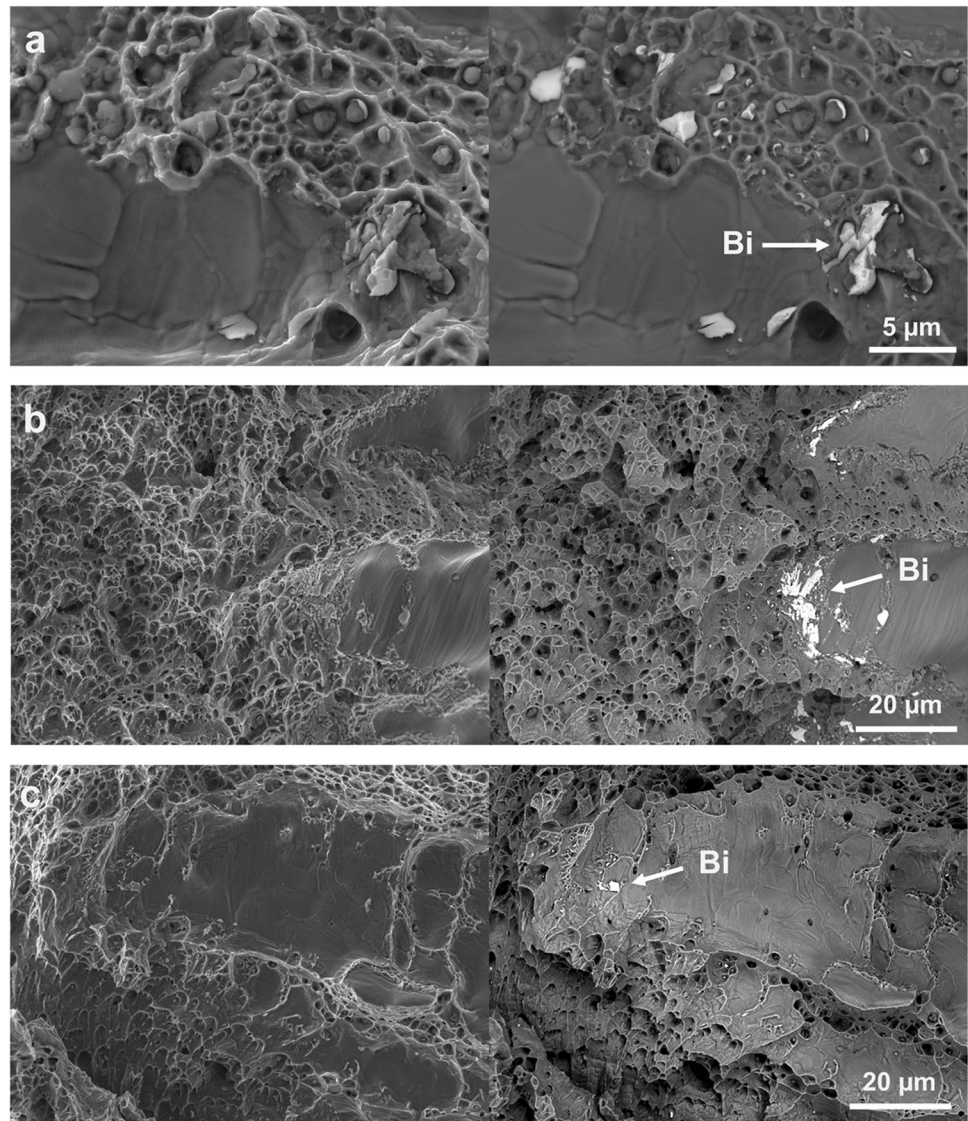
A correlation between the weld metal oxygen content and the solidification cracking susceptibility was not evident as cracks were detected in the T0 wires with both the highest and lowest levels, 0.088 and 0.062 wt.-%, respectively. It is, however, possible that oxygen as surface active element affects the solidification range and that a difference could be observed if all wires would originate from the same source.

It is well known that the weld metal oxygen content also affects the impact toughness [25–27]. In this work, the measured range was 0.050–0.088 wt.-% and the regular T1 wires mostly resulted in an oxygen content of 0.060–0.065 wt.-%. Deviations were, however, observed for wires from different manufacturers. The impact toughness of the T0 wire with the highest oxygen content of 0.088 wt.-% was in the same range as another wire with 0.062 wt.-%. The bismuth-free wires of T1 type generally showed the highest impact toughness, but the oxygen content varied from 0.050 to 0.083 wt.-%. This altogether indicates that the selection of raw materials by various formulators may be decisive. The T0 wires generally contain SiO_2 to optimize the performance for down hand welding. With additions of quartz, more Bi_2O_3 is typically added to improve the weld bead shape and slag removal. This leads to increased levels of oxygen as compared to the T1 wires with more rutile in the flux. As the T1 wires contain less SiO_2 and more TiO_2 to allow for welding in all positions, less Bi_2O_3 is required for proper slag detachability. The goal with this paper was, however, not to reveal differences in flux compositions between different manufacturers.

4.2 Ferrite content and cracking

A requirement of the phase balance is common for welding procedures when welding duplex stainless steels. The ferrite content in the weld metal is normally specified at 30–70% [32] or stricter with 35–65% [33–36]. Neither the measured (31–64 FN) nor calculated ferrite content (35–64 FN) could

Fig. 4 Bright phase identified as bismuth present in the flat region of hot cracks observed on fracture surfaces on impact toughness samples for the wires. **a** E2209T0-G, **b** E2209T0-E, **c** E2209T1-A (left SE, right BSE)



be correlated to the cracking susceptibility. An analysis of the chemical composition of all-weld metal and certificates from the various manufacturers of the different flux-cored wires showed no consistent relationship among the ferrite-forming alloying elements chromium, molybdenum, and silicon, nor the austenite stabilizing nickel, manganese, and nitrogen on the presence of cracks.

The advantage with primary ferritic solidification in austenitic weld metal has been suggested to be greater solubility of harmful elements and that the total amount of grain boundaries becomes larger [37]. As shown in Fig. 11a–b, the ferrite grain boundaries in the duplex welds are rather long and straight [19]. This resembles more the grain boundary conditions in fully austenitic welds than those of the standard austenitics with a few percent ferrite [38]. Yu et al. [39] have suggested that coarse and long dendrites having straight boundaries could help liquid

films remain continuous and allow cracks to propagate. Suutala et al. [40] concluded that in welds exhibiting 30% ferrite, interdendritic liquid films would be more likely to wet the ferrite/ferrite boundaries. Depending on the resulting brittle temperature range of low-melting films and the solidification range of the slag, the duplex alloys may become more susceptible to solidification cracking. Matsuda et al. [6] studied duplex stainless steels and observed a higher degree of microsegregation in the higher temperature range and that the number of inclusions gradually increased with the ferrite content. It was concluded that the risk for hot cracking was higher with a lower liquation temperature, but the large grain size of these alloys with only 0.09–0.12 wt.-% nitrogen may also have contributed.

All wires showed primary ferritic solidification as indicated by the calculated FN using WRC'92. Upon cooling, the austenite first precipitates in the grain boundaries and

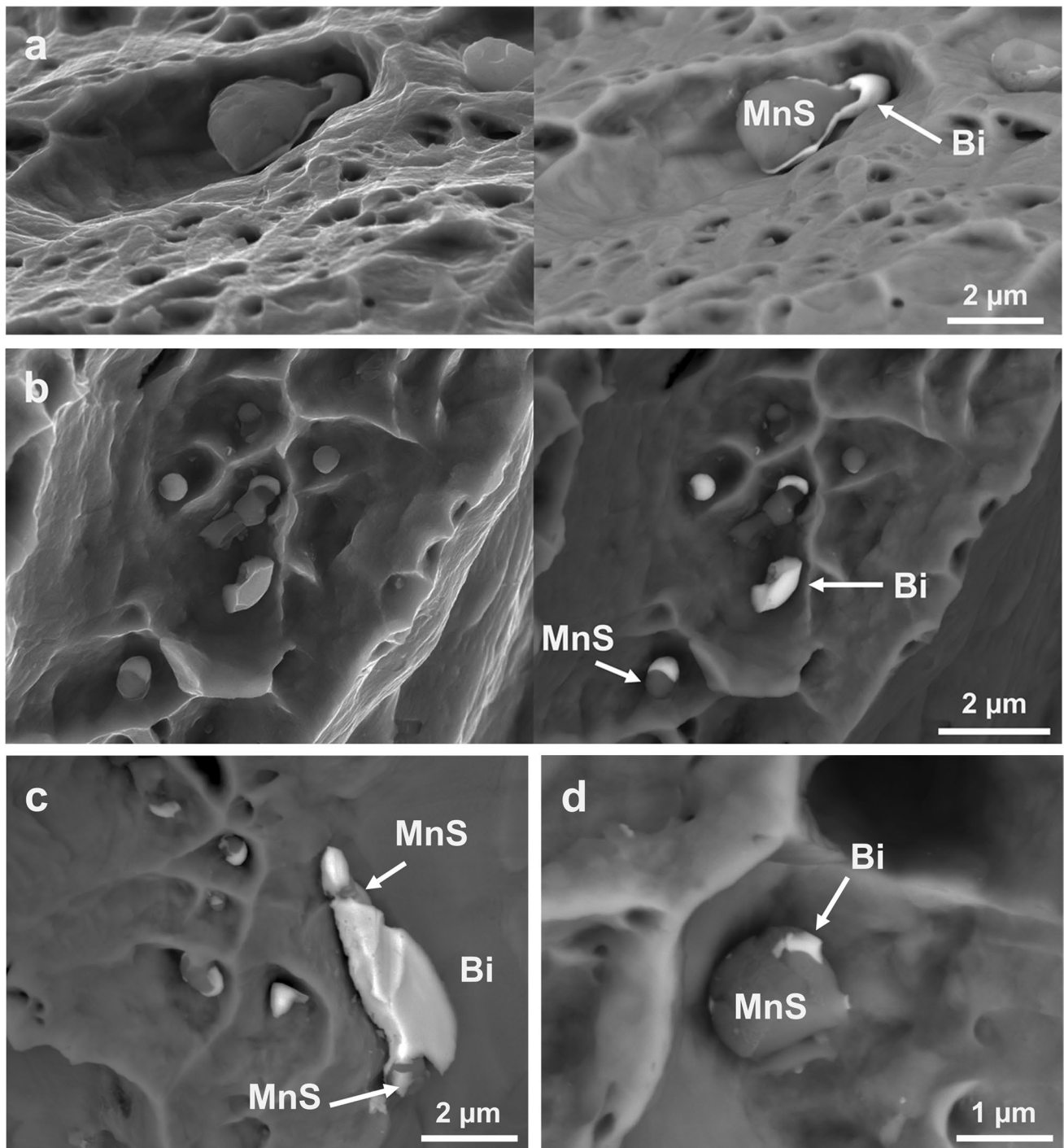


Fig. 5 Dark phase consisting of MnS and bright phase identified as bismuth present in the flat region with the wires **a** E2209T0-G (left SE, right BSE), **b** E2209T0-E (left SE, right BSE), **c** E2209T1-A (BSE), and **d** E2209T1-A (BSE)

then grows through diffusion of primarily nitrogen. In the previous generations of duplex stainless steels, the nitrogen content was considerably lower. This resulted in highly ferritic weld metal microstructures with precipitates such as chromium nitrides and carbides, and limited amounts of austenite mainly found in the grain boundaries [7, 8].

With the modern wires, the driving force for austenite formation is higher, promoting growth of both grain boundary and Widmanstätten austenite. The older generations of duplex stainless steels rarely showed any cracking [18]. There is a possibility that the improved austenite formation has increased the sensitivity to solidification cracking

Fig. 6 Small bright areas of bismuth on MnS in dimples on the fracture surface with wires. **a** E2209T0-H and **b** E2209T1-B (left SE, right BSE)

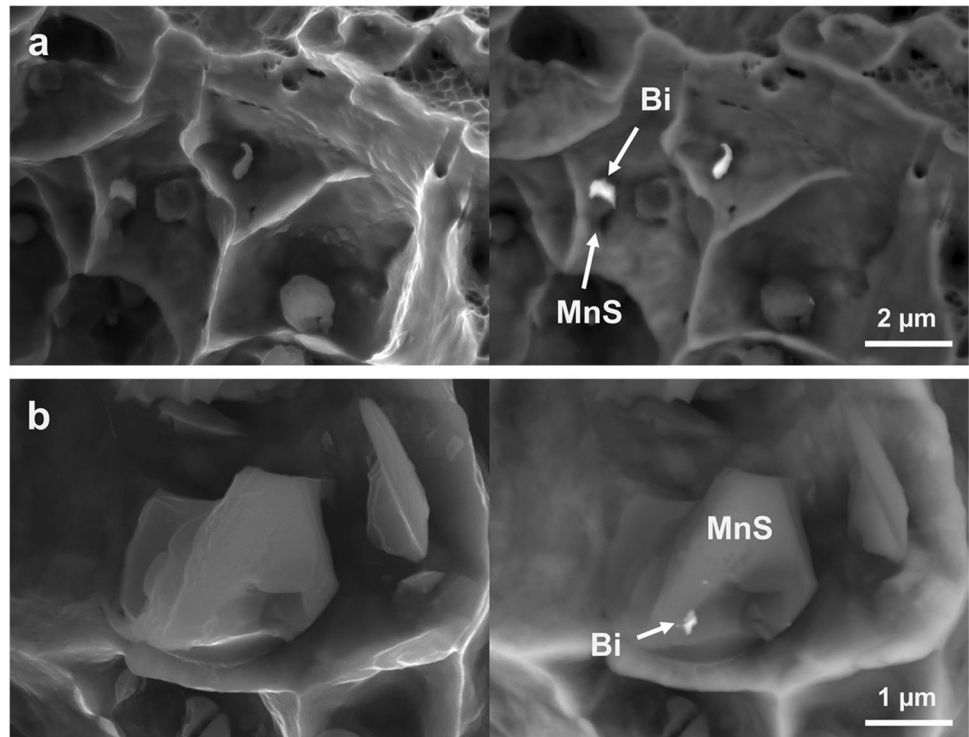
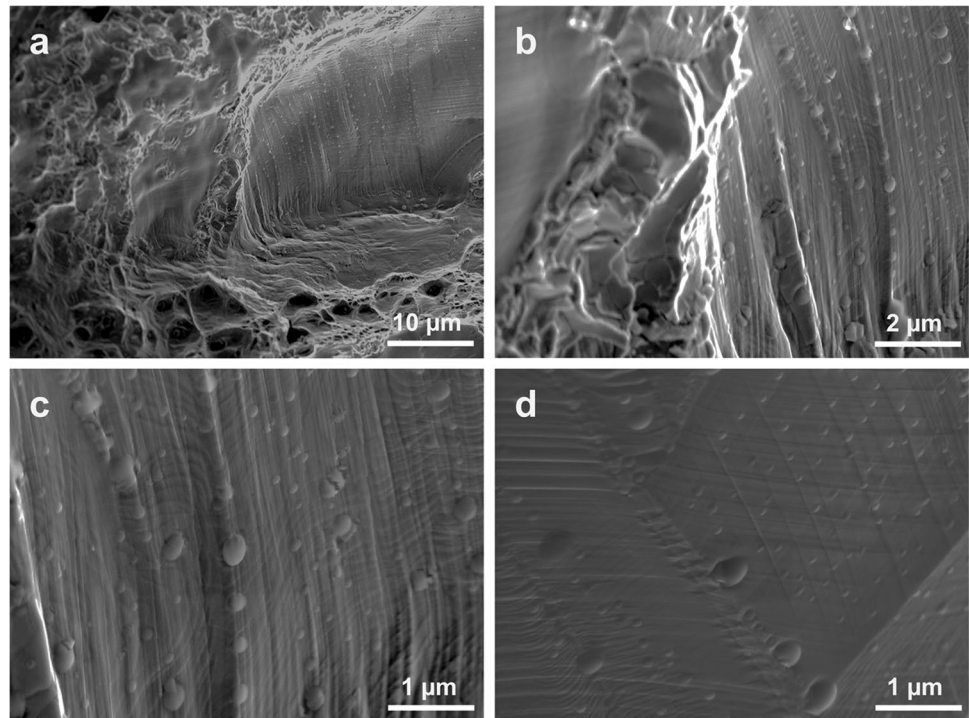


Fig. 7 Spherical particles located on the solidification crack surface of wire E2209T1-Q (in-Beam SE) **a** overview, **b** higher magnification, **c** particles along striations, and **d** larger particles located in dendrite and grain boundaries



as the austenite does not as efficiently dissolve impurities as ferrite and parts of the low-melting phases located in the grain boundaries are probably still molten when all austenite has formed.

Modern alloys with nitrogen additions have, in addition, higher strength than the older generations of duplex

stainless steels and fillers. This can increase the susceptibility to solidification cracking due to exposure to higher strain and strain rates [2, 12, 15, 41, 42]. The difference in strength between the E2209T0 and E2209T1 wires is low, however, and would not explain the observed differences in weldability.

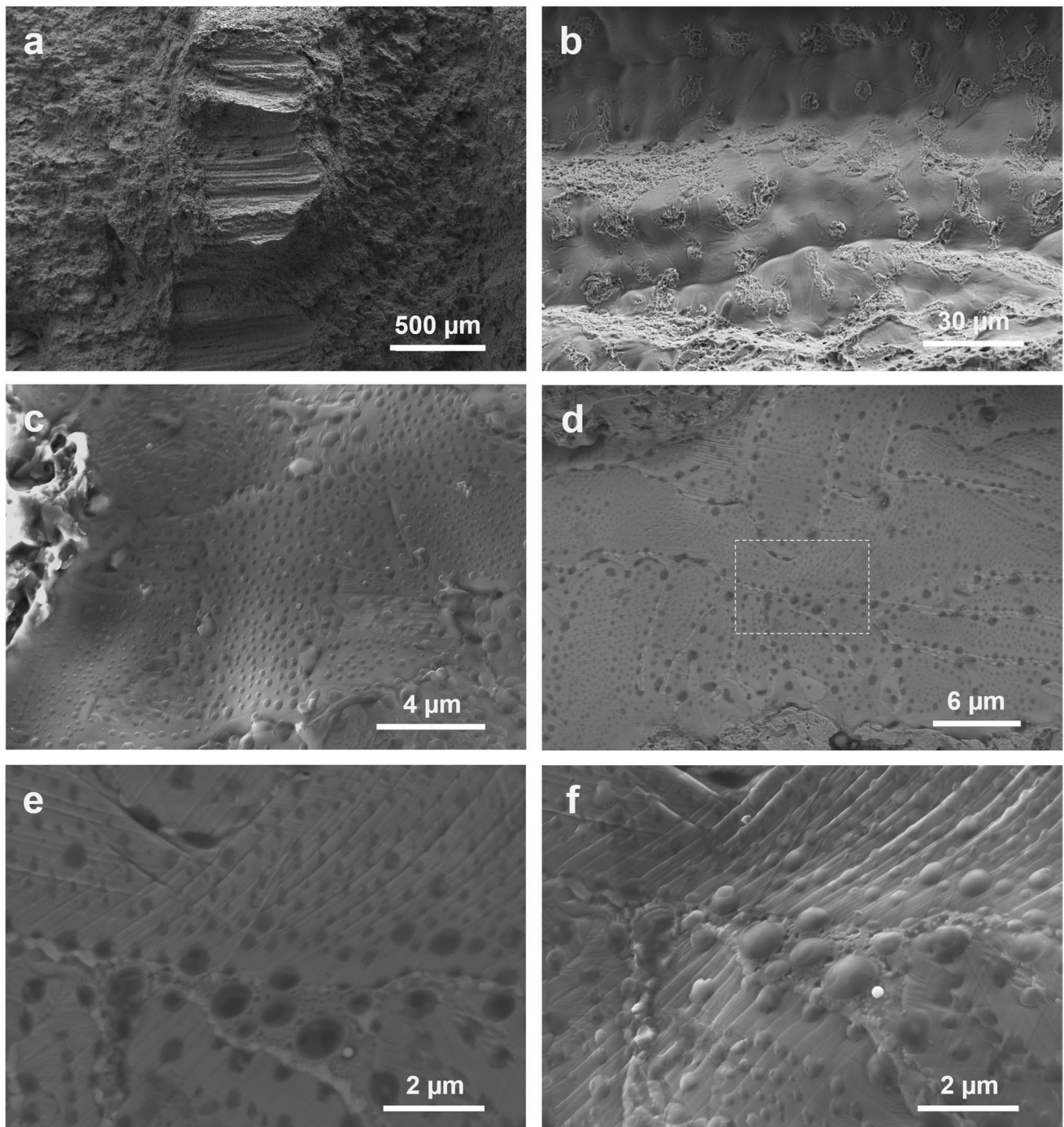


Fig. 8 **a** Solidification crack found on the fracture surface of an impact toughness sample welded with wire E2209T1-Q (SE) with **b** dendritic solidification pattern in the crack (SE), **c** particles at the very surface of the solidification crack (inLens SE detector), **d** dendritic solidification fingers growing from different sides with smaller round particles in the dendrite core and larger round particles close to

the boundaries (BSE), **e** striation lines, grain boundary precipitates, small surface particles decorating the complete surface (inLens SE detector), **f** smaller dark particles in the center, larger dark particles close to the boundaries, and a single bright particle of essentially pure molybdenum (BSE)

4.3 Restraint and welding parameters

Kou [43] stated that the risk for hot cracking is determined

by the solidification temperature range, the amount and distribution of liquid at the terminal stage of solidification, the surface tension of the grain-boundary liquid, the ductility of

Fig. 9 Dimples with particles found on the fracture surfaces with (a) wire E2209T1-P and (b) wire E2209T1-R (SE)

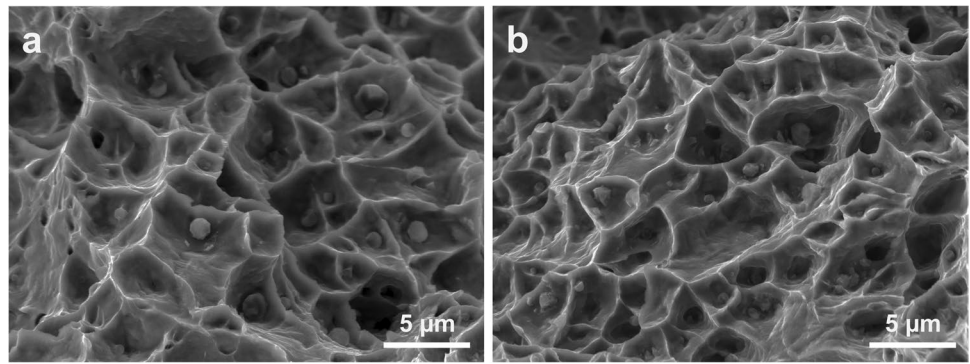


Fig. 10 Effect of the phosphorous, sulfur, bismuth, and boron content in the all-weld metal on the impact toughness at $-40\text{ }^{\circ}\text{C}$

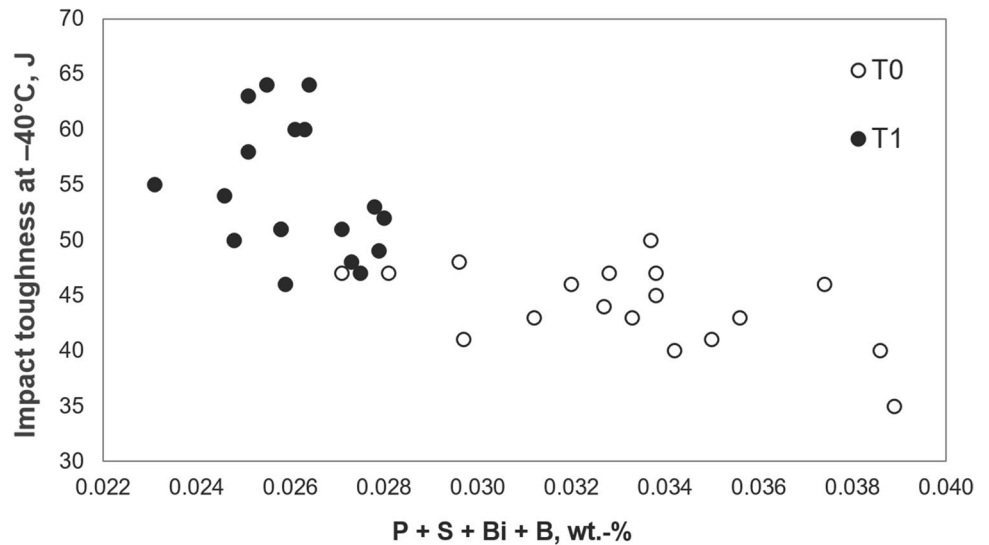
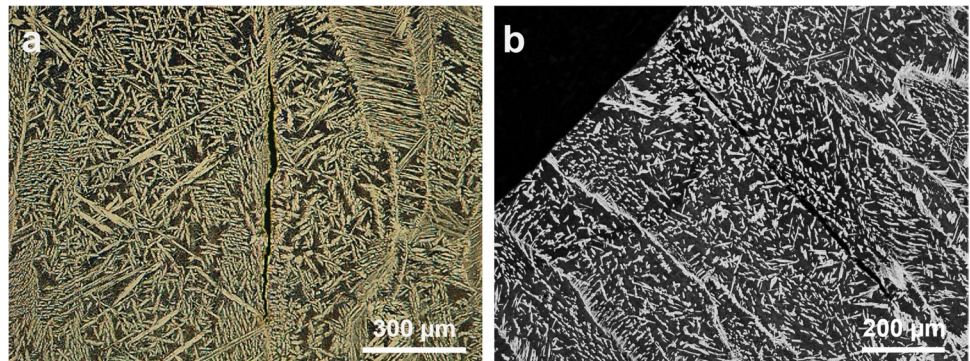


Fig. 11 a UNS S32205 plate welded in a V-joint with an E2209T0 wire showing a crack in the center of the weld bead (10% NaOH) and (b) crack in a UNS S32205 fillet weld welded with an E2209T0 wire (Beraha II) [19]



solidifying weld metal, and the tendency for weld metal contraction and the degree of restraint. Duplex stainless steels have higher strength than the austenitics and it has been concluded that these grades also can experience problems in highly restrained constructions [7, 12, 15, 41]. In rare cases, preheating of the base material to maximum $150\text{ }^{\circ}\text{C}$ can minimize the risk of cracking when welding thick and/or heavily restrained work pieces with low arc energy to reduce cooling rate and stress levels [15]. In the present work, steel

plates were welded to the plates to prevent distortion and the mild steel plates and backing were preheated to $100\text{ }^{\circ}\text{C}$. Hence, high restraint could be obtained and the possible positive effect of preheating included.

The various wires show different weldability and may allow or force the welder to weld slightly in another way. With the manual welding performed in this work, there may have been small variations in welding speed, stick-out, arc length, and gun manipulation. This affects the shape of the

weld puddle and possible nitrogen absorption. Mechanized welding would be needed to eliminate this potential variable.

4.4 Scanning electron microscopy (SEM)

The cracks seen on fracture surfaces showed typical dendritic solidification patterns (Fig. 1). This is the result of liquid films having a lower melting point than the rest of the weld, and the thermal strain associated with welding that opens up the melt into a crack [43]. As dendrites are formed in the solidifying melt, cellular-dendrite primary and secondary arms are typically visible on the crack surface.

Matsuda et al. [5, 44, 45] divided the fracture surface morphology of hot cracks formed in fully austenitic SUS 310S and fully ferritic SUS 430 into the three different regions — dendritic, dendritic-flat, and flat — while the austenitic SUS 304 showed dendritic morphology only [5]. The solidification was suggested to go from dendritic to flat as the temperature decreased and the size of the smooth area increased with strain and strain rate. Katayama et al. [38] studied stainless alloys with different solidification modes and observed that when the solidification was fully ferritic, the crack surface showed both dendritic and flat regions. In Part 1 of this work [19], the same phenomenon was observed for solidification cracks formed in flux-cored arc welds in UNS S32101 and UNS S32205.

The cracks observed with SEM in this work primarily consisted of a dendritic-flat region where primary arms dominated the surface, while the area identified as the tip of the crack was rather flat. On the flat crack surface and in surrounding dimples, particles could often be found due to potentially higher concentration in the last solidified melt (Figs. 2, 3 and 4). Matsuda et al. [45] suggested that the liquid film covers all the grain boundary for dendritic and dendritic-flat areas, resulting in lower ductility than in the flat region where solid bridging starts. The smooth surface was proposed to be the result of lower amounts of phosphide-type liquid phase and that the crack passes through the migrating grain boundary.

Bismuth was most easily visualized in an SEM using backscatter mode, in which it became brighter than the matrix (Figs. 2, 3 and 4). When found, the element was present not only in the flat region of the solidification cracks, but also in dimples surrounding the crack and in smaller quantities in the dimples in both unaffected areas and crack-free samples. Lower amounts of iron, chromium, manganese, and sulfur could also be detected in bismuth-rich areas. Due to a peak overlap for molybdenum ($\text{Mo } L_{\alpha,\beta}$) and sulfur ($\text{S } K_{\alpha}$), it is not possible to unambiguously assign and quantify these elements. The complexity was increased as the fillers are alloyed with 3 wt.-% molybdenum while sulfur mainly is a trace element (0.002–0.007 wt.-%). Nonetheless, bismuth in its liquid

phase appears to be present in close proximity to MnS and preferentially wet the surface of these particles (Fig. 3).

It is suggested that both sulfur and bismuth form low-melting phases that can be found in the last solidifying melt in the grain boundaries, but that bismuth has a lower solidification temperature than MnS and thus stays molten. Bismuth has been reported to lead to efficient wetting of grain boundaries and dendrites [46]. This is also a possible reason why bismuth is found primarily in the crack tip with the last solidified melt. In the samples without hot cracks, less sulfur and bismuth were detected in the dimples with SEM/EDS. The size of the MnS particles remained in the same range, but fewer particles were observed.

The E2209T0 wires generally contained more bismuth and sulfur than the E2209T1 wires. It needs to be emphasized that a few bismuth-free wires of E2209T1 type were subject to solidification cracking, while some wires with higher sulfur contents were not. Here, the slag concepts among different manufacturers may, to various extents, play a role and make the weld metal more or less tolerant.

The bismuth-free wire E2209T1-Q has, according to the manufacturer, improved impact toughness, and this could be confirmed with an average of 78 J at room temperature and 60 J at -40°C . The fracture surfaces and SEM investigation, however, confirmed solidification cracking (Figs. 5 and 6). The sulfur content was the second highest for all T1 wires and some MnS formation was confirmed, but another observed phenomenon is suggested to be decisive.

Many aligned particles could be observed within dendrites and at dendrite and grain boundaries (Figs. 5 and 6). These decorated the entire surface following the segregation pattern; being smaller interdendritically and larger closer to the boundaries indicating precipitation in the structure as the solidification front progressed. The size was in the range 0.09–1.2 μm with the largest particles found in the ferrite grain boundaries. The MnSi-rich particles are suspected to originate from the flux and it is also possible that there was some contamination with sulfur and/or phosphorus. The fact that the manganese silicates remain intact suggests that these are distributed in the dendrites on solidification and can be a factor in the liquid film failure. Cardoso Junior et al. [31] also found MnSi-oxides with some traces of titanium and aluminum in multipass flux-cored arc welds using an E2209T1 type wire. It may be possible to improve the cracking resistance of E2209T1-Q by substituting the raw material(s) forming manganese silicates.

The flat region of the crack surface was observed to have striations similar to those previously seen in austenitic stainless steels and nickel-base alloys [47, 48]. The striations form in the solid-state and the fact that they are oriented differently in various grains possibly reflects the difference in crystal orientation among adjacent grains [49]. This type of appearance is typically observed for ductility dip

cracking, but the crack start here showed dendritic solidification. Some striations were present in the solidification cracks in other samples, but for all these, primary dendrites were clearly visible. As also stated for the wires in Part 1 [19], all solidification cracks were already present in the underlying weld beads and there were no signs of liquation cracking.

The type of oxide inclusions and particles found on the fracture surface and in the dimples on ductile surfaces can affect the cracking susceptibility. Kou [42] stated that cracking may be initiated at metastable pore nuclei, oxide films, or gas trapped in the vicinity of oxides. Due to the alloying of duplex grades with nitrogen, the risk may increase as compared to the standard austenitics. In Part 1 [19], pores were observed at the crack start of welds produced with a flux-cored wire of E2307T0 type. Srivastava et al. [50] suggest that larger inclusions nucleate voids at relatively small strains and smaller particles nucleate voids at much larger strains. The size of the void nucleating particles is typically between 0.1 and 100 μm , with volume fractions of no more than a few percent. Large inclusions have, in addition, been reported to serve as initiation of pitting [51, 52]. The unaffected fracture surfaces in this work showed a typical structure of ductile duplex welds [53, 54]. Fine dimples contained particles of 0.1–0.3 μm and larger 0.5–3.0 μm . Dimples mostly contain inclusions of some type. Arun et al. [55] showed oxides in dimples on fracture surfaces of E2209T1 welds and concluded that these were enriched in iron, manganese, silicon, chromium, and titanium. Gupta et al. [56] welded UNS S32750 superduplex stainless steel with E2595 covered electrodes and the particles found in dimples on fracture surfaces were rich in iron, manganese, chromium, molybdenum, and silicon. Zhang et al. [57] found silicon, manganese, and titanium-rich oxide inclusions and smaller Si–C–O inclusions in dimples in E2209T0 type flux-core wire arc additive manufacturing.

Although the wires contained higher contents of phosphorous than sulfur, no phosphorous could be detected with EDS. This is in agreement with the work of Katayama et al. [38] who found both sulfides and phosphides with austenitic solidification and only sulfides when the solidification was fully ferritic. The absence of phosphorous can, however, also be related to the type of analysis and does not automatically mean that phosphorous did not affect the cracking susceptibility. In Part 1 [19], a bismuth particle cross-sectioned by means of focus ion beam (FIB) and examined with transmission electron microscopy (TEM)/EDS showed higher concentrations of lead, sulfur, and phosphorous. Lippold and Savage [58] suggested that phosphorous in hot cracks found on polished surfaces was preferably measured using electron microprobe analysis (EPMA). Matsuda et al. [45] studied solidification cracks formed in transverse testing of austenitic SUS 310S with 0.003–0.092 wt.-% phosphorous and 0.004–0.062 wt.-% sulfur using SEM/EDS and EPMA.

Both phosphides and sulfides were found in the solidification cracks, and it was suggested that the sulfides had already solidified in the flat mode, while phosphorous would still be liquid. Phosphorous may thus significantly contribute to the crack susceptibility.

4.5 Bismuth

Most flux-cored wires contain around 0.02 wt.-% (200 ppm) bismuth to improve the slag removal and promote clean weld surfaces [59]. Reports of intergranular cracking and premature creep failure in austenitic welds after a period of service at 650–825 °C have concluded that bismuth segregates on the dendrite or grain boundaries at elevated temperatures, which affects the creep ductility and resistance to reheat cracking [28–30, 60–62]. AWS A5.22 [63] states that stainless steel electrodes containing bismuth additions should not be used for high-temperature service or post-weld heat treatment (PWHT) above about 900°F (500 °C) and it became mandatory in 2012 to report the content if bismuth is intentionally added, or if it is known to be present at levels greater than 0.002%. API [64] has incorporated a limit of 20-ppm bismuth in austenitic stainless steel FCAW deposits, when these weld metals are exposed to temperatures above 1000°F (538 °C) during PWHT or during service. EN ISO 17633 [20] from 2017 only mentions that bismuth should be restricted to 20 ppm maximum for alloys intended for high-temperature service.

Bismuth has in the present work mainly been identified as particles on the fracture surface or as coating of MnS than as grain boundary films, although it is likely that the intergranular compounds were impurity enriched liquid films at higher temperature. The EDS spectra all showed some carbon and oxygen contents indicating that there was some surface contamination or oxidation. The carbon peak was considerably more prominent than the oxygen peak. Hence, the oxygen content was not sufficiently high to indicate that bismuth was present as bismuth oxide Bi_2O_3 . In creep and embrittlement studies of austenitic FCAW weld metal containing bismuth, segregation has been observed in the grain boundaries with a particle-like distribution without any clear relation to oxygen [27, 62]. This is of importance as the melting point for bismuth oxide Bi_2O_3 is 830 °C, while pure bismuth melts already at 270 °C [62]. Instead, it is suggested that bismuth is present as bismuth phase coating or adhering to MnS. Similar observations have been made by Melford [65], who reported that lead is present in the crack surfaces of austenitic stainless steels as globules of elemental lead, often associated with MnS particles and not as grain boundary films.

Impurities that segregate at the grain and solidification boundaries have historically also been reported to decrease the hot workability of austenitic stainless steel; lead and

bismuth are especially harmful, but tin, antimony, and arsenic have also been pinpointed [1, 12, 46, 66–69]. Globular particles of essentially pure lead have also been detected in the grain boundaries at high temperatures by other scientists [70–72]. Apart from possibly bismuth, none of these elements is included in the standard analysis and the accuracy and reproducibility may vary between different laboratories [73].

Bismuth has been reported to be more detrimental than lead due to more efficient wetting of grain boundaries and dendrites [46]. The face-centered cubic structure of austenite is more sensitive to wetting of the boundaries than the body-centered cubic structure of ferrite. This may be of significance as the low-melting films responsible for solidification cracking may still be liquid at the temperatures where grain boundary austenite has precipitated in long and straight ferrite grain boundaries [19].

Due to the risk of 475 °C embrittlement, duplex stainless steels are rarely used at service temperatures exceeding 250 °C and for this low temperature, no negative influence of bismuth on cracking sensitivity has been reported. It is, however, known that addition of bismuth oxide, Bi_2O_3 , has a measurable somewhat negative effect on the impact toughness in austenitics [27, 29, 30, 72].

Hara et al. [30] investigated the effect of small amounts of bismuth in the weld metal on the corrosion resistance and found no effect of retained bismuth in the 308 type FCAW weld metal as compared to bismuth-free GTAW and SMAW weld metal. On contrary, Ogawa et al. [74] have suggested that bismuth in duplex flux-cored wires has a negative effect on the corrosion resistance. The mechanism was not clarified, but the authors recommend that the use of bismuth should be limited to 0.015 wt.-%. As the ASTM G48 pitting corrosion test also exposes the end grains to the FeCl_3 solution, small solidification cracks of the type found in this work may serve as initiation points for pitting and add to the measured weight loss. This may be one explanation why Ogawa et al. [74] reported that bismuth lowers the corrosion resistance of duplex stainless steel welded with flux-cored wire. Sugahara et al. [75] stated that preferably the use of Bi_2O_3 should be limited to 0.005 wt.% in duplex stainless steel flux-cored wires, but gave no further information on why this limit was selected. This specific value could not be confirmed in this work, but if concentrating on one slag base only, it may be possible to determine a recommended maximum value. The wires examined ranged from bismuth-free up to 0.011 wt.-% bismuth and the average bismuth addition was 0.004 wt.-%. No clear correlation could be found between the amount and the cracking susceptibility — a few bismuth-free wires cracked, while some wires with higher bismuth content did not. To specify bismuth-free flux-cored wires for welding duplex stainless steels would thus not be necessary, but careful wire selection and qualification of

the welding procedures are recommended. The T1 wires were either bismuth-free or contained 0.002 wt.-% bismuth. There was a fairly small variation in bismuth content, but the impact toughness showed up to 20-J difference. It should be mentioned that a completely bismuth-free composition also could have a negative influence on the slag removal and weld shape and require more post weld cleaning work. This is a possible reason why no manufacturer offers bismuth-free wires of T0 type.

4.6 Effect of chemical composition of flux-cored wires

When comparing the flux-cored wires from the different manufacturers, it is evident that there are fairly large variations in the composition, but all were well within the standards EN ISO 17633 and AWS A5.22. Also, the ferrite content in the final weld bead measured with FeriteScope® would meet most specifications.

Flux-cored wires consist of a sheath metal and elements for alloying, slag forming, and deoxidation are added through the flux. Unlike solid wires, the difference between various manufacturers is considerable with different concepts. Depending on the philosophy of the producer, there can be substantial deviations in intensity, arc stability, and slag formation [76]. Different slags can have better desulfurizing activity [77, 78] and prevent loss of alloying elements such as manganese and silicon [79]. The raw materials may come from the same sources, but the selection of type, content, and size of the flux components can be quite different. Heat-to-heat variations may occur based on strip material heats, but also different lots of each and every raw material added to the flux. Often, the formulists need to balance the recipe to achieve an attractive surface appearance with good slag removal without having a negative effect on the impact toughness. Zhang et al. [80] reported that the impact toughness decreased in superduplex welds when the pitting corrosion resistance increased. A flux-cored wire is consequently always a compromise.

Segregation of impurities and alloying elements are suggested to induce the solidification cracking found in the duplex all-weld metal. The low-melting phases concentrated in the grain boundaries are still liquid when being subjected to the strain formed in the weldment. The long and straight ferrite grain boundaries allow propagation of cracks once initiated [5, 19, 38]. The range of the typical alloying elements and impurities affecting the hot cracking susceptibility was rather wide for the different wires in this work. The total amount of bismuth, sulfur, phosphorous, boron, and oxygen was considerably higher in the wires of E2209T0 type, but it was not possible to unambiguously label any as clearly unfavorable, and the E2209T1 wires in particular appeared rather unaffected by higher content of a single element. This does

not mean that these elements do not affect the solidification cracking sensitivity, but that the difference between the E2209T0 and E2209T1 types and the diverse slag concepts by various manufacturers may be dominating [76].

Although it is well known that sulfur and phosphorous are generally negative for the hot cracking resistance of stainless steels, these elements cannot be completely avoided in flux-cored wires due to some amounts in the strip material, but also as contamination of other raw materials. In addition, very low sulfur contents may affect the weld bead penetration, fluidity of the weld metal, and possibly the slag detachability.

Sulfur was detected as granular MnS particles in dimples and solidification cracks on the fracture surface. Small amounts of globular MnS have previously been found in both austenitic SUS 304 and fully austenitic SUS 310S weld metals containing 0.003–0.005 wt.-% sulfur [81], SUS 310S with 0.014 wt.-% sulfur [45], and duplex SUS 329J2L with 0.006–0.008 wt.-% sulfur [6]. Yamada et al. [81] recommend limiting the sulfur content to maximum 0.0050 wt.-%. In the present work, it was not possible to state the critical limit to avoid solidification cracking, but it should be aimed to keep the total amount of impurities down. MnS has also been reported to serve as pitting initiation in austenitic stainless steels [82–84].

To optimize the weld bead shape and slag removal, the slag of the down hand E2209T0 wires for welding in the best position is designed to be more fluid and for a longer period of time. The slag coating formed with the all-position E2209T1 wires, on the other hand, should solidify considerably faster to allow for welding in the vertical up and overhead positions. This has been shown in detail in the work by Holly et al. [76], where the viscosities of the slag of austenitic stainless flux-cored wires of E308LT0 and E308LT1 type were correlated with differential thermal analysis. The controlled solidification is obtained by changing the slag formulation, often by a reduction of silica, SiO₂, and increased amounts of rutile, TiO₂, and zirconia, ZrO₂.

It has been suggested that a reduction of the solidification temperature range may improve the resistance to hot cracking [5], but it is not clear how much the slag solidification rate contributes. For cracks located close to the surface, it is possible that the additional cooling from a faster solidified slag could have a slightly positive effect on the susceptibility. In general, the E2209T1 types showed the highest impact toughness and resistance to solidification cracking. When found, the cracks were typically few and short. Visual inspection of the crack surfaces showed dendritic solidification and regardless of wire type, the primary dendrite arm spacing (pDAS) became wider as the cracks grew. In the beginning of the crack where the surface was dendritic or dendritic flat, the pDAS was slightly narrower for the E2209T1 (Fig. 3c–d) than the E2209T0 wires (Fig. 3a–b). The flat region where the last solidified melt was present,

however, became rather wide for all wire types (Fig. 4 and Fig. 7a). Close to the weld bead surface, the slag formation rate may influence the threshold of liquid phases needed for crack formation and the final crack size, but most likely the concentration of impurities and the resulting amounts of low-melting phases present in the ferrite grain boundaries become decisive. An E2209T1 wire would thus be inherently less sensitive to formation of cracks than an E2209T0 with more impurities and higher oxygen levels. Although specific products from certain manufacturers may perform better than others, the general recommendation for welding thick standard duplex plates under high restraint would be to apply a flux-cored wire of E2209T1 type.

5 Summary

Different E2209T0 and E2209T1 duplex stainless steel flux-cored wires from various manufacturers have been examined for the suitability of welding thick material under high restraint. Welding of fully restrained plates is associated with an increased risk of cracking, but the conditions accurately reflect many of the applications where these types of wires are already used. All-weld metal samples were subjected to impact toughness testing and the fracture surfaces inspected. The chemical composition of all tested wires was well within the limits set for E2209TX-X in AWS A5.22 and T 22 9 3 N L in EN ISO 17633. No relationship between the measured ferrite content in the last weld bead and the cracking susceptibility could be found.

Irregularities examined by means of SEM/EDS showed dendritic surfaces typical for solidification cracking, with a transition from dendritic-flat to flat morphology. Bismuth particles were visible at the flat end of the cracks, especially in back-scatter mode. These were found adhered to MnS or as a partial coating of MnS particles indicating that bismuth was the last element to solidify. As cracking was observed with wires without bismuth or with fairly low sulfur content, the phenomenon could not be explained by these elements only. The occurrence of solidification cracks was more frequent in E2209T0, while very few and mostly only small cracks were found when welding with the all-position E2209T1 wires. The E2209T1 wires generally showed the highest impact toughness and resistance to solidification cracking and would thus be preferred for welding of thick-walled duplex stainless steels. The main reason for the better performance is suggested to be the lower total content of impurities combined with a slag system containing more rutile, TiO₂, which substantially reduces the slag solidification temperature range.

Acknowledgements The authors want to thank welding companies, distributors, and filler wire producers for sharing their experience in

solidification cracking of duplex welds and for providing various flux-cored wires. Dipl.-Ing. Andrea Putz at TU Graz (now at Andritz AG Group), Prof. John C. Lippold at The Ohio State University, and Prof. Carl E. Cross at Los Alamos National Laboratory are acknowledged for valuable discussions. The contribution from Andrea Maderthoner at voestalpine Böhler Welding and the team of Global R&D Joining Cored Wires for wire development and testing is highly appreciated. Michael Reischl at voestalpine Forschungsservicegesellschaft Donawitz GmbH assisted with SEM/EDS work. Prof. Norbert Enzinger at TU Graz and Dr. Thomas Willidal at voestalpine Böhler Welding were part of the FFG Green Welding project team. Yngve Axelsson at Jernkontoret, Sweden, provided some of the older papers and reports.

Author contribution Dr. Elin Marianne Westin collected the wires, performed the welding tests and involved experimental work, did the literature review, developed some of the wire formulations, and wrote the paper. Dr. Fernando Gustavo Warchomicka operated the SEM and provided the EDS measurement data. Both authors have read and agreed to the published version of the manuscript.

Funding The SEM work at TU Graz was financed by Die Österreichischer Forschungsförderungsgesellschaft project “FFG Green Welding.”.

Declarations

Conflict of interest The authors declare no competing interests.

References

- Ogawa T, Koseki T (1989) Effect of composition profiles on metallurgy and corrosion behavior of duplex stainless steel weld metals. *Weld J Res Suppl* 68(5):181–191. http://files.aws.org/wj/supplement/WJ_1989_05_s181.pdf
- Coniglio N, Cross CE (2013) Initiation and growth mechanism for weld solidification cracking. *Int Mat Rev* 58(7):375–397. <https://doi.org/10.1179/1743280413Y.0000000020>
- Coniglio N, Cross CE (2009) Mechanisms for solidification crack initiation and growth in aluminum welding. *Metall Mater Trans A* 40(11):2718–2728. <https://doi.org/10.1007/s11661-009-9964-4>
- Castro R, de Cadenet JJ (1974) *Welding metallurgy of stainless and heat-resisting steels*. Cambridge University Press, Cambridge
- Matsuda F, Nakagawa H, Uehara T, Katayama S, Arata Y (1979) A new explanation for role of delta-ferrite improving weld solidification cracks susceptibility in austenitic stainless steel. *Transactions of JWRI* 8(1):105–112. <http://hdl.handle.net/11094/5579>
- Matsuda F, Nakagawa H, Kato I, Murata Y (1986) Solidification crack susceptibility in weld metals of duplex stainless steels. *Transactions of JWRI* 15(1):99–112 <http://hdl.handle.net/11094/10729>. Accessed on December 28, 2021
- Nelson DE, Baeslack WA III, Lippold JC (1987) An investigation of weld hot cracking in duplex stainless steels. *Weld J Res Suppl* 66(8):241s–250s
- Varol I, Baeslack WA III, Lippold JC (1989) Characterization of weld solidification cracking in a duplex stainless steel. *Metallography* 23(1):1–19. [https://doi.org/10.1016/0026-0800\(89\)90037-2](https://doi.org/10.1016/0026-0800(89)90037-2)
- Gooch TG (1983) Weldability of duplex ferritic-austenitic stainless steels. *Proc. Duplex Stainless Steels '82*. St Louis, Mo, ASM, Metals Park, Ohio, Paper 8201–029:573–602
- Honeycombe J, Gooch TG (1977) Intergranular attack in welded stress-corrosion resistant stainless steel. *Weld J Res Suppl* 56(11):339s–353s
- Brooks JA, Lambert FJ Jr (1978) The effects of phosphorous, sulfur and ferrite content on weld cracking of type 309 stainless steel. *Weld J Res Suppl* 57(5):139s–143s
- Lippold JC, Kotecki DJ (2005): *Welding metallurgy and weldability of stainless steels*. John Wiley & Sons, Inc., New Jersey. 376pp. ISBN: 978–0–471–47379–4
- Shankar V, Gill TPS, Mannan SL, Sundaresan S (2003) Solidification cracking in austenitic stainless steel welds. *Sadhana* 28(3–4):359–382
- Saida K, Ogura T (2018) Hot cracking susceptibility in duplex stainless steel welds. *Mater Sci Forum* 941(12):679–685. <https://doi.org/10.4028/www.scientific.net/MSF.941.679>
- Karlsson L (2012) Welding duplex stainless steels – a review of current recommendations. *Weld World* 56(3):65–76. <https://doi.org/10.1007/BF03321351>
- Fellman A, Westin EM (2008) Fiber laser hybrid welding of stainless steels. *Proc. ICALEO® Congress Materials Processing Conference, Temecula, CA. Paper #1204:545–553*
- Cross CE, Coniglio N, Westin EM, Gumenyuk A (2011) Laser weldability of stainless steel. Hot cracking phenomena in welds III, Springer-Verlag Berlin and Heidelberg GmbH & Co. K, Berlin, Germany, 131–144. ISBN: 9783642168635
- Westin EM (2022) Hot cracking in duplex stainless steel weldments – a review. *Weld World* 66(8):1483–1449, 1450–1451. <https://doi.org/10.1007/s40194-022-01310-8>, <https://doi.org/10.1007/s40194-022-01338-w>
- Westin EM, Putz A, Maderthoner A, Pilhagen J (2022) Solidification cracking in duplex stainless steel flux-cored arc welds Part 1 – Cracking in 30-mm-thick material welded under high restraint. Accepted for publication in *Welding in the World*. <https://doi.org/10.1007/s40194-022-01370-w>
- EN ISO 17633 Welding consumables – tubular cored electrodes and rods for gas shielded and non-gas shielded metal arc welding of stainless and heat-resisting steels – classification (2018) European Committee for Standardization, Brussels, Belgium. 46pp.
- ISO 15792–1 (2020) Welding consumables – Test methods. Part 1: Preparation of all-weld metal test pieces and specimens in steel, nickel and nickel alloys. European Committee for Standardization, Brussels, Belgium. 20pp.
- EN ISO 17655 (2003) Destructive tests on welds in metallic materials – method for taking samples for delta ferrite measurement. European Committee for Standardization, Brussels, Belgium, pp 11
- ISO 148–1 (2017) Metallic materials – Charpy pendulum impact test Part 1: test method. European Committee for Standardization, Brussels, Belgium. 42pp.
- ISO 17781 (2017) Petroleum, petrochemical and natural gas industries – test methods for quality control of microstructure of ferritic/austenitic (duplex) stainless steels. European Committee for Standardization, Brussels, Belgium. 34pp.
- Ekström U, Olsson K (1980) The influence of ferrite and oxygen contents on weld metal mechanical properties of submerged-arc welded stainless steels. *Proc. Weld Pool Chemistry and Metallurgy, TWI, London. UK Paper 37:323–331*
- Holmberg B (1997) How to perform welding in duplex stainless steels to obtain optimum weld metal properties. *Stainless Steel World* 3:28–33
- Westin EM, Schnitzer R, Ciccomascolo F, Maderthoner A, Grönlund K, Runnsjö G (2016) Austenitic stainless steel bismuth-free flux-cored wires for high-temperature applications. *Weld World* 60(6):1147–1158. <https://doi.org/10.1007/s40194-016-0376-y>
- Tsukimoto K, Toyoda M, Matsumoto O, Kawaguchi S (1998) Effect of elements on weldability and hot ductility of FCAW stainless steel weld metal. *Weld World* 41(3):240–252. Pergamon Press. ISSN: 0043–2288

29. Nishimoto K, Matsunaga T, Tanaka T, Okazaki T (1998) Effect of bismuth on reheat cracking susceptibility in type 308 FCAW weld metal. *Weld World* 41:220–235. Pergamon Press. ISSN: 0043–2288
30. Hara Y, Shiga K, Nakazawa N (2002) Effects of small amount of bismuth on corrosion resistibility of austenitic stainless steel weld metals. *Proc. PVP2002 ASME Pressure Vessels and Piping Conference, Vancouver, BC, Canada*, 4pp.
31. Cardoso Junior R, Bracarense AQ, Campos FR, Souza CS, Silveira DM, Lins VFC (2012) Evaluation of multipass welding of thick lean duplex stainless steel UNS S32304 plates welded by SMAW, GMAW and FCAW – part I: mechanical properties. *Soldag Insp* 17(4):306–316 (in Portuguese) <https://doi.org/10.1590/S0104-92242012000400005>
32. EN ISO 15156–3 (2020) Petroleum and natural gas industries – materials for use in H₂S-containing environments in oil and gas protection. Part 3: cracking-resistant CRAs (corrosion resistant alloys) and other alloys. European Committee for Standardization, Brussels, Belgium. 80pp.
33. Gunn RN (1997) Duplex stainless steels: microstructure, properties and applications. Woodhead Publishing Ltd, Cambridge
34. Karlsson L (2000) Welding of stainless steels. Duplex and superduplex steels *Weld Int* 14(12):5–11. <https://doi.org/10.1080/09507110009549131>
35. Berglund G, Wilhelmsson P (1989) Fabrication and practical experience of duplex stainless steels. *Mater Des* 10:23–28
36. Knyazeva M, Pohl M (2013) Duplex steels: part I: genesis, formation, structure. *Metallogr Microstruct Anal* 2(4):113–121. <https://doi.org/10.1007/s13632-013-0066-8>
37. Arata Y, Matsuda F, Katayama S (1976) Solidification crack susceptibility in weld metals of fully austenitic stainless steels (report I): fundamental investigation on solidification behavior of fully austenitic and duplex microstructures and effect of ferrite on microsegregation. *Transactions of JWRI* 5(2):35–51. <http://hdl.handle.net/11094/7813>
38. Katayama S, Fujimoto T, Matsunawa A (1985) Correlation among solidification process, microstructure, microsegregation and solidification cracking susceptibility in stainless steel weld metals (materials, metallurgy & weldability). *Transactions of JWRI* 14(1):123–138. <http://hdl.handle.net/11094/10942>
39. Yu P, Thompson KJ, McCarthy J, Kou S (2018) Microstructure evolution and solidification cracking in austenitic stainless steel welds. *Weld J Res Suppl* 97(9):301s–314s
40. Suutala N, Takalo T, Moiso T (1979) Austenitic solidification mode in austenitic stainless steel welds. *Metall Trans A* 10(8):1183–1190. <https://doi.org/10.1007/BF02811664>
41. Liljas M (1995) The welding metallurgy of duplex stainless steels, *Proc. Duplex Stainless Steels '94, Glasgow, Scotland, Vol. 2:Paper KV:15pp*.
42. Kou S (2015) A simple index for predicting the susceptibility to solidification cracking. *Weld J Res Suppl* 94(12):374s–388s
43. Kou S (2003) Solidification and liquation cracking issues in welding. *JOM* 55(6):37–42. <https://doi.org/10.1007/s11837-003-0137-4>
44. Arata Y, Matsuda F, Nakagawa H, Katayama S, Ogata S (1977) Solidification crack susceptibility in weld metals of fully austenitic stainless steels (Report III): effect of strain rate on cracking threshold in weld metal during solidification. *Transactions of JWRI* 6(2):37–46. <http://hdl.handle.net/11094/9667>
45. Matsuda F, Nakagawa H, Ogata S, Katayama S (1978) Investigation on solidification crack in the Vareststraint test of fully austenitic stainless steel – studies on fractography of welded zone (III). *Transactions of JWRI* 7(1):59–70 <http://hdl.handle.net/11094/10586>. Accessed on June 19, 2022
46. Jensfeld PM, Norrman TO (1962) Bismuth and its effect on hot workability of stainless steel. *Jernkontor Annlr* 146(6):438–452
47. DuPont JN, Lippold JC, Kiser SD (2009) *Welding metallurgy and weldability of nickel-base alloys*. John Wiley & Sons, Inc. 440pp. <https://doi.org/10.1002/9780470500262>
48. Lippold JC (2015) *Welding metallurgy and weldability*. John Wiley & Sons, Inc. 400pp. <https://doi.org/10.1002/9781118960332>
49. Lippold JC (2021) Private communication
50. Srivastava A, Ponson L, Osovski S, Bouchaud E, Tvergaard V, Needleman A (2014) Effect of inclusion density on ductile fracture toughness and roughness. *J Mech Physics* 63(2):62–79. <https://doi.org/10.1016/j.jmps.2013.10.003>
51. Sicupira DC, Frankel GS, Lins VFC (2016) Pitting corrosion of welds in UNS S32304 lean duplex stainless steel. *Mater Corros* 67(5):440–448. <https://doi.org/10.1002/maco.201508502>
52. Zhang Z, Jing H, Xu L, Han Y, Zhao L (2017) Influence of microstructure and elemental partitioning on pitting corrosion resistance of duplex stainless steel welding joints. *Corros Sci* 394(2):194–210. <https://doi.org/10.1016/j.apsusc.2016.10.047>
53. Kokawa H, Umeda S, Kuwana T (1994) Effects of nitrogen on tensile properties of duplex stainless steel weld metal. *Weld Int* 8(6):531–537. <https://doi.org/10.1080/09507119409548630>
54. Hu Y, Shi Y-H, Shen X-Q, Wang Z-M (2017) Microstructure, pitting corrosion resistance and impact toughness of duplex stainless steel underwater dry hyperbaric flux-cored arc welds. *Materials* 10(1443):18. <https://doi.org/10.3390/ma10121443>
55. Arun D, Ramkumar D, Vimala R (2019) Multi-pass welding techniques of 12 mm thick super-duplex stainless steel. *J Mat Proc Tech* 271(5):126–143. <https://doi.org/10.1016/j.matprotec.2019.03.031>
56. Gupta A, Kumar A, Baskaran T, Arya SB, Khatirkar RK (2018) Effect of heat input on microstructure and corrosion behavior of duplex stainless steel shielded metal arc welds. *Trans Indian Inst Met* 71(7):1595–1606. <https://doi.org/10.1007/s12666-018-1294-z>
57. Zhang Y, Cheng F, Wu S (2021) The microstructure and mechanical properties of duplex stainless steel components fabricated via flux-cored wire arc-additive manufacturing. *J Manuf Process* 69(9):204–214. <https://doi.org/10.1016/j.jmapro.2021.07.045>
58. Lippold JC, Savage WF (1982) Solidification of austenitic stainless steel weldments: part III – the effect of solidification behavior on hot cracking susceptibility. *Weld J Res Suppl* 62(12):388s–396s
59. Farrar JCM, Marshall AW, Zhang Z (2001) Position statement on the effect of bismuth on the elevated temperature properties of flux cored stainless steel weldments. *Weld World* 45(5/6):25–31
60. Chemical Plant Welding Research Committee of the Japan Engineering Society (JWES) (1996) High temperature damage to stainless steel welds made by flux-cored arc welding and its analysis. *Proc. API 61th Fall Refinery Meeting*, pp. 21–23
61. Nishiyama S, Matsushita Y, Maruyama T (1995) Flux-cored wires for stainless steel welding. *Weld World* 36(6):103–123. Pergamon Press. ISSN: 0043–2288
62. Konosu S, Hashimoto A, Mashiba H, Takeshima T, Ohtsuka T (1998) Creep crack growth properties of type 308 austenitic stainless steel weld metals. *Weld J Res Suppl* 77(8):22s–327s
63. AWS A5.22/A5.22M (2012) Specification for stainless steel flux cored and metal cored welding electrodes and rods. A8.1.4 Bismuth (Bi) in flux cored stainless steel electrodes. American Welding Society, Miami, FL, USA, pp 55
64. American Petroleum Institute Recommended Practice, API RP 582 (2009) *Welding guidelines for the chemical, oil, and gas industries*, 2nd edition, American Petroleum Institute, Washington, DC, USA, pp 14
65. Melford DA (1980) The influence of residual and trace elements on hot shortness and high temperature embrittlement. *Phil Trans R Soc Lond A* 295(1413):89–101

66. Myllykoski L, Suutala N (1983) Effect of solidification mode on hot ductility of austenitic stainless steels. *Met Technol* 10(1):453–460. <https://doi.org/10.1179/030716983803291307>
67. Ljungström LG (1977) Influence of trace elements on the hot ductility of austenitic 17Cr13NiMo-steel. *Scand J Metall* 6:176–184
68. Norström L-Å (1979) A comment on the influence of trace elements on the hot ductility of austenitic 17Cr 13Ni Mo-steel. *Scand J Metall* 8(2):95–96
69. Skoglund E (1979) Inverkan av föroreningar på rostfria ståls varmbearbetbarhet. Jernkontorets forskningsuppgift, Internal report JK 493/73 (in Swedish)
70. Walsh JM, Anderson NP (1976) Characterization of nickel-base superalloy fracture surfaces by Auger electron spectroscopy. *Proc. Superalloys Seven Springs Conference, AIME/TMS*:127–136
71. Bergh S (1949) Influence of lead on behavior of stainless steel. *Iron Age* 164(14/7):96–99; *Met Rev* 22(9):32
72. Tsukimoto K, Tozoda M, Marsumoto O, Kawaguchi S (1998) Effect of elements on weldability and hot ductility of FCAW stainless steel weld metal. *Weld World* 41:240–252
73. Kotecki DJ (2014) Round robin of trace elements. *Weld World* 58(4):577–592. <https://doi.org/10.1007/s40194-014-0147-6>
74. Ogawa T, Maruyama T, Ozaki S (2002) Flux cored wire for welding duplex stainless steel. United States Patent US 6,340,396 B1. 12pp.
75. Sugahara H, Ikeda T, Watanabe H (2010) Flux-cored wire for stainless steel arc welding. United States Patent Application Publication US 2011/0139761 A1. 9pp.
76. Holly S, Mayer P, Bernhard C, Posch G (2018) Slag characterisation of 308L-type stainless steel rutile flux-cored wires. *Weld World* 63(2):293–311. <https://doi.org/10.1007/s40194-018-0675-6>
77. Brown SD, Roxburgh RJ, Ghita I, Bell HB (1982) Sulphide capacity of titania-containing slags. *Ironmaking Steelmaking* 9(4):163–167
78. Iwamoto N (1982) Structure of slag (X) – desulfurization. *Transactions of JWRI* 11(2):155–163. <http://hdl.handle.net/11094/4344>
79. Iwamoto N (1983) Structure of slag (XI) – role of TiO₂ in slag. *Transactions of JWRI* 12(1):131–141. <http://hdl.handle.net/11094/8829>
80. Zhang Z, Golding M, van der Mee V (2018) Pitting corrosion resistance properties of super duplex stainless steel weld metals and influencing factors. *Weld World* 63(3):663–672. <https://doi.org/10.1007/s40194-018-00684-y>
81. Matsuda F, Katayama S, Arata Y (1981) Solidification crack susceptibility in weld metals of fully austenitic stainless steels (report V): solidification crack susceptibility and amount of phosphide and sulfide in SUS 310S weld metals. *Transactions of JWRI* 10(2):73–84. <http://hdl.handle.net/11094/11708>
82. Wijesinghe TSL, Blackwood DJ (2007) Real time pit initiation studies on stainless steels: the effect of sulphide inclusions. *Corros Sci* 49(4):1755–1764. <https://doi.org/10.1016/j.corsci.2006.10.025>
83. Schmuki P, Hildebrand H, Friedrich A, Virtanen S (2005) The composition of the boundary region of MnS inclusions in stainless steel and its relevance in triggering pitting corrosion. *Corros Sci* 4(5):123–125. <https://doi.org/10.1016/j.corsci.2004.05.023>
84. Stewart J, Williams DE (1992) The initiation of pitting corrosion on austenitic stainless steel: on the role and importance of sulphide inclusions. *Corros Sci* 33(2):457–474. [https://doi.org/10.1016/0010-938X\(92\)90074-D](https://doi.org/10.1016/0010-938X(92)90074-D)

Publisher's note Springer Nature remains neutral with regard to jurisdictional claims in published maps and institutional affiliations.

Springer Nature or its licensor holds exclusive rights to this article under a publishing agreement with the author(s) or other rightsholder(s); author self-archiving of the accepted manuscript version of this article is solely governed by the terms of such publishing agreement and applicable law.